CrystEngComm

Accepted Manuscript

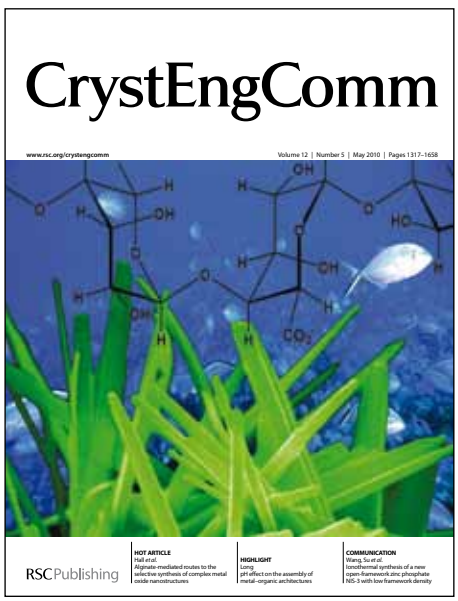

CrystEngComm

Dynamic Article Links ▶

Cite this: DOI: 10.1039/c0xx00000x

www.rsc.org/CrystEngComm

ARTICLE

Syntheses, Structures, and Properties of A Series of 2D and 3D Coordination Polymers Based on Trifunctional Pyridine-dicarboxylate and Different (Bis)imidazole Bridging Ligands

Liming Fan,[a] Xiutang Zhang,[*a,b] Wei Zhang,[b] Yuanshuai Ding,[b] Weiliu Fan,[a] Liming Sun,[a] Xian Zhao[*a]

Received (in XXX, XXX) Xth XXXXXXXXX 2013, Accepted Xth XXXXXXXXX 2013
DOI: 10.1039/c0xx00000x

ABSTRACT: A series of 2D and 3D transition coordination polymers (CPs), $\{[M(bcpb)(1,4\text{-bmib})_{0.5}]\cdot xH_2O\}_n$ (M = Co (**1**), Cu (**2**), Ni (**3**), x= 1 for **1**, 0 for **2** and **3**), $\{[Co(bcpb)(4,4'\text{-bibp})_{0.5}(H_2O)_{1.5}]\cdot 1.5H_2O\}_n$ (**4**), $[Cu(bcpb)(4,4'\text{-bibp})_{0.5}(H_2O)]_n$ (**5**), $\{[Ni(bcpb)(4,4'\text{-bimbp})(H_2O)]\cdot 2.5H_2O\}_n$ (**6**), $[Co(bcpb)(4,4'\text{-bimbp})]_n$ (**7**), $[Mn(pip)(MeOH)(H_2O)]_n$ (**8**), $\{[Ni(pip)(4,4'\text{-bibp})_{0.5}(H_2O)]\cdot 2H_2O\}_n$ (**9**), and $\{[Cu(pip)(4,4'\text{-bimbp})]\cdot 4H_2O\}_n$ (**10**), were synthesized under hydrothermal conditions in the presence of two trifunctional pyridine-dicarboxylate and different (bis)imidazole bridging linkers (H_2bcpb = 3,5-bis(4-carboxyphenyl)pyridine, H_2pip = 5-(4-pyridyl)-isophthalic acid, 1,4-bmib = 1,4-bis(2-methylimidazol-1-ylmethyl)benzene), 4,4'-bibp = 4,4'-bis(imidazol-1-yl)biphenyl, 4,4'-bimbp = 4,4'-bis(imidazol-1-ylmethyl)biphenyl). Their structures have been determined by single-crystal X-ray diffraction analyses and further characterized by elemental analyses, IR spectra, powder X-ray diffraction (PXRD), and thermogravimetric (TG) analyses. Single crystal X-ray diffraction analyses reveal that complexes **1-3** are isomorphic and show complicated 3D (3,5)-coordinated **amd** networks, which could be viewed as two interpenetrated **ths** nets. Complex **4** is a binodal (3,4)-connected 3D framework with the Schläfli symbol of $(4\cdot7^2)(4\cdot7^5\cdot8^4)$. Complex **5** exhibits an intriguing 3D 2-fold interpenetrated network with the (3,4)-connected **dmc** net. Complex **6** is a 2D (3,5)-connected **gek1** net with right- and left-handed $[Ni(4,4'\text{-bibp})]_n$ helix chains arranged alternately. The 3D framework of **7** is defined as a 2-fold interpenetrated (3,5)-connected **gra** topology. Complex **8** displays a 2D 3-connected 6^3-**hcb** network. Complex **9** can be regard as a (3,4)-coordinated **crs-d** network with point symbol of $(6^2\cdot8)(6^3\cdot8\cdot10^2)$, which contains two interpenetrated 3-coordinated 10^3 **srs** subnets linked by 2-coordinated 4,4'-bibp. Complex **10** is a binodal (3,5)-connected 3D framework with point Schläfli symbol of $(4\cdot6\cdot8)(4\cdot6^4\cdot8^5)$. To the best of our knowledge, the 3D CPs with (3,4)-connected $(4\cdot7^2)(4\cdot7^5\cdot8^4)$ for **4**, and (3,5)-connected $(4\cdot6\cdot8)(4\cdot6^4\cdot8^5)$ for **10** have never been documented up to now. Moreover, the magnetic property of **4** has been investigated.

Introduction

The design and synthesis of coordination polymers (CPs) have attracted upsurging research interest not only because of their diverse structures and intersting topologies but also owing to their tremendous potential applications in gas storage,[1a-d] microelectronics,[1e] ion exchange,[1f,1g] chemical separations,[2a-c] nonlinear optics,[2d,2e] drug delivery,[2f] molecular magnetism,[3a-c] photoluminescence,[3d,3e] and heterogeneous catalysis.[3f] Generally, the structural diversity of such materials are always dependent on many factors, such as metal ion,[4a,4b] templating agents,[4c,4d] metal-ligand ratio,[4e] pH value,[5a,5b] counteranion,[5c] and number of coordination sites provided by organic ligands.[5d,5e] In the strategies, the rational selection of organic ligands or coligands according to their length, rigidly, coordination modes, functional groups is one of the most important strategies for the assembly of structural controllable CPs, and a great deal of significant work have been done by using the strategy.[6]

Usually, the polycarboxylate ligands with bent backbones, such as V-shaped, triangular, quadrangular, and so on, are excellent candidates for building highly connected, interpenetrating, or helical coordination frameworks due to their bent backbones and versatile bridging fashions.[7,8] Among which, trifunctional pyridine-dicarboxylic acids are paid much attention due to their rich donor atoms including N and O atoms. 3,5-bis(4-carboxyphenyl)pyridine (H_2bapb) and 5-(4-pyridyl)-isophthalic acid (H_2pip) have been used in the assembly of functional coordination polymers, which revealed diverse structures and excellent properties.[9] Apart from the polycarboxylate linkers, (bis)imidazole bridging linkers are frequently used in the assembly process of coordination

[a] *State Key Laboratory of Crystal Materials, Shandong University , Jinan 250100, China.*
E-mail: *zhaoxian@icm.sdu.edu.cn.*
[b] *Advanced Material Institute of Research, College of Chemistry and Chemical Engineering, Qilu Normal University, Jinan, 250013, China.*
E-mail: xiutangzhang@163.com.

†Electronic Supplementary Information (ESI) available: Additional Figures, IR spectrum, Powder XRD patterns and X-ray crystallographic data, CCDC 932484-932490 for **1-7**, CCDC 949697-949699 for **8-10**. See DOI: 10.1039/c0xx00000x.

polymers act as bridging pillars, guest molecules, or charge balance roles.[10] Moreover, the (bis)imidazole bridging linkers also play important role on altering the coordination modes of polycarboxylate ligands.[11] The particular behaviors allow them to be promising candidates for designing frameworks with diverse topologies.[12]

On the basis of above-mentioned considerations and followed our recent research,[13] we consider the simultaneous employment of two trifunctional pyridine-dicarboxylate (H_2pip, H_2bcpb) and three (bis)imidazole bridging linkers (1,4-bmib, 4,4'-bibp, and 4,4'-bimbp) (Scheme 1) with different length (l_p) and width (l_c) will contribute to the formation of various architectures and help chemists understand the process of self-assembly. Herein, we successfully apply this strategy and obtain ten 2D and 3D CPs, namely, $\{[M(bcpb)(1,4\text{-}bmib)_{0.5}]\cdot xH_2O\}_n$ (M = Co (**1**), Cu (**2**), Ni (**3**), x= 1 for **1**, 0 for **2** and **3**), $\{[Co(bcpb)(4,4'\text{-}bibp)_{0.5}(H_2O)_{1.5}]\cdot 1.5H_2O\}_n$ (**4**), $[Cu(bcpb)(4,4'\text{-}bibp)_{0.5}(H_2O)]_n$ (**5**), $\{[Ni(bcpb)(4,4'\text{-}bimbp)(H_2O)]\cdot 2.5H_2O\}_n$ (**6**), $[Co(bcpb)(4,4'\text{-}bimbp)]_n$ (**7**), $[Mn(pip)(MeOH)(H_2O)]_n$ (**8**), $\{[Ni(pip)(4,4'\text{-}bibp)_{0.5}(H_2O)]\cdot 2H_2O\}_n$ (**9**), and $\{[Cu(pip)(4,4'\text{-}bimbp)]\cdot 4H_2O\}_n$ (**10**), which exhibit a systematic variation of architectures from 2D layers to 3D frameworks. These results reveal that not only the length (l_p) and width (l_c) of the trifunctional pyridine-dicarboxylate ligands but also the flexibility and length of the (bis)imidazole bridging linkers have great effect on the final packing structures.

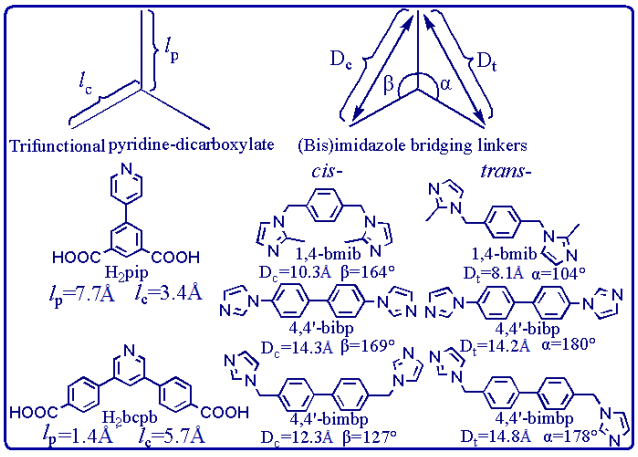

Scheme 1. Structural characteristics of two trifunctional pyridine-dicarboxylate (H_2pip, H_2bapb) and (bis)imidazole bridging linkers (1,4-bmib, 4,4'-bibp, and 4,4'-bimbp).

Experimental Section

Materials and Physical Measurements. The syntheses of **1**–**10** were performed in Teflon-lined stainless steel autoclaves under autogenous pressure. The chemicals of 5-(4-pyridyl)-isophthalic acid, 3,5-bis(4'-carboxyphenyl)pyridine, 1,4-bis(2-methylimidazol-1-ylmethyl)benzene, 4,4′-bis(1-imidazolyl)biphenyl, and 4,4'- bis(imidazol-1-ylmethyl)biphenyl were purchased from Jinan Henghua Sci. & Tec. Co. Ltd. without further purification. IR spectra were measured on a Nicolet 740 FTIR Spectrometer at the range of 400-4000 cm^{-1}. Elemental analyses were carried out on a CE instruments EA 1110 elemental analyzer. TGA was measured from 25 to 800 °C on a SDT Q600 instrument at a heating rate 5 °C/min under the N_2 atmosphere (100 mL/min). X-ray powder diffractions were measured on a Panalytical X-Pert pro diffractometer with Cu-Kα radiation. The variable-temperature magnetic susceptibility measurements was performed on the Quantum Design SQUID MPMS XL-7 instruments in the temperature range of 2-300 K under a field of 1000 Oe.

General Synthesis Procedure for Complexes 1–10. The synthesis for the target ten complexes were performed in 25 mL Teflon-lined stainless steel vessels by utilizing the hydrothermal method with the same stoichiometric ratio for the starting materials in the presence of NaOH. The one-pot mixture was heated to 170 °C for 72 h, and then cooled to room temperature at a descent rate of 10 °C/h. Finally, the crystals suitable for the single-crystal X-ray diffraction analysis were obtained.

Synthesis of $\{[Co(bcpb)(1,4\text{-}bmib)_{0.5}]\cdot H_2O\}_n$ (1). A mixture of H_2bcpb (0.20 mmol, 0.064 g), 1,4-bmib (0.20 mmol, 0.054 g), cobalt(II) dichloride hexahydrate (0.20 mmol, 0.048 g), NaOH (0.30 mmol, 0.012 g), and 12 mL H_2O was placed in a Teflon-lined stainless steel vessel, heated to 170 °C for 3 days, followed by slow cooling (a descent rate of 10 °C/h) to room temperature. Purple block crystals of **1** were obtained. Yield of 59% (based on Co). Anal. (%) calcd. for $C_{54}H_{42}Co_2N_6O_9$: C, 62.56; H, 4.08; N, 8.11. Found: C, 62.37; H, 4.21; N, 7.98. IR (KBr pellet, cm^{-1}): 3453 (s), 3081 (m), 2370 (m), 1601 (vs), 1534 (vs), 1401 (vs), 1223 (m), 847 (m), 763 (s), 517 (w).

Synthesis of $[Cu(bcpb)(1,4\text{-}bmib)_{0.5}]_n$ (2). A mixture of H_2bcpb (0.20 mmol, 0.064 g), 1,4-bmib (0.40 mmol, 0.108 g), copper(II) sulfate pentahydrate (0.40 mmol, 0.100 g), NaOH (0.30 mmol, 0.012 g), and 12 mL H_2O was placed in a Teflon-lined stainless steel vessel, heated to 170 °C for 3 days, followed by slow cooling (a descent rate of 10 °C/h) to room temperature. Blue block crystals of **2** were obtained. Yield of 43% (based on Cu). Anal. (%) calcd. for $C_{27}H_{20}CuN_3O_4$: C, 63.09; H, 3.92; N, 8.18. Found: C, 62.73; H, 3.97; N, 8.67. IR (KBr pellet, cm^{-1}): 3461 (s), 3083 (m), 2369 (m), 1597 (vs), 1543 (vs), 1398 (s), 1230 (m), 851 (m), 767 (m), 521 (w).

Synthesis of $[Ni(bcpb)(1,4\text{-}bmib)_{0.5}]_n$ (3). A mixture of H_2bcpb (0.20 mmol, 0.064 g), 1,4-bmib (0.20 mmol, 0.054 g), nickel(II) sulfate hexahydrate (0.50 mmol, 0.141 g), NaOH (0.30 mmol, 0.012 g), and 12 mL H_2O was placed in a Teflon-lined stainless steel vessel, heated to 170 °C for 3 days, followed by slow cooling (a descent rate of 10 °C/h) to room temperature. Green block crystals of **3** were obtained. Yield of 67% (based on Ni). Anal. (%) calcd. for $C_{27}H_{20}N_3NiO_4$: C, 63.69; H, 3.96; N, 8.25. Found: C, 64.01; H, 3.67; N, 8.36. IR (KBr pellet, cm^{-1}): 3457 (s), 3083 (m), 2367 (s), 1611 (vs), 1538 (vs), 1407 (s), 1220 (m), 853 (m), 764 (s), 523 (w).

Synthesis of $\{[Co(bcpb)(4,4'\text{-}bibp)_{0.5}(H_2O)_{1.5}]\cdot 1.5H_2O\}_n$ (4). A mixture of H_2bcpb (0.20 mmol, 0.064 g), 4,4′-bibp (0.20 mmol, 0.057 g), cobalt(II) nitrate hexahydrate (0.20 mmol, 0.058 g), NaOH (0.30 mmol, 0.012 g), and 12 mL H_2O was placed in a Teflon-lined stainless steel vessel, heated to 170 °C for 3 days, followed by slow cooling (a descent rate of 10 °C/h) to room temperature. Pink block crystals of **4** were obtained. Yield of 49% (based on Co). Anal. (%) calcd. for $C_{112}H_{94}Co_4N_{12}O_{27}$: C, 59.11; H, 4.16; N, 7.39. Found: C, 58.91; H, 4.23; N, 7.17. IR

(KBr pellet, cm^{-1}): 3434 (s),3087 (m), 2371 (m), 1607 (vs), 1567 (m), 1397 (vs), 1290 (m), 1102 (m), 799 (m), 753 (m), 522 (w).

Synthesis of $[Cu(bcpb)(4,4'\text{-bibp})_{0.5}(H_2O)]_n$ (5). A mixture of H_2bcpb (0.20 mmol, 0.064 g), 4,4'-bibp (0.20 mmol, 0.057 g), copper(II) sulfate pentahydrate (0.20 mmol, 0.050 g), NaOH (0.30 mmol, 0.012 g), and 12 mL H_2O was placed in a Teflon-lined stainless steel vessel, heated to 170 °C for 3 days, followed by slow cooling (a descent rate of 10 °C/h) to room temperature. Blue block crystals of **5** were obtained. Yield of 37% (based on Cu). Anal. (%) calcd. for $C_{28}H_{20}CuN_3O_5$: C, 62.05; H, 3.72; N, 7.75. Found: C, 61.89; H, 4.04; N, 7.48. IR (KBr pellet, cm^{-1}): 3445 (vs), 3118 (m), 2373 (m), 1605 (vs), 1567 (s), 1398 (vs), 1311 (s), 875 (m), 790 (m), 531 (w).

Synthesis of $\{[Ni(bcpb)(4,4'\text{-bimbp})(H_2O)]\cdot 2.5H_2O\}_n$ (6). A mixture of H_2bcpb (0.20 mmol, 0.064 g), 4,4'-bimbp (0.20 mmol, 0.053 g), nickel(II) sulfate hexahydrate (0.20 mmol, 0.057 g), NaOH (0.30 mmol, 0.012 g), 12 mL H_2O was placed in a Teflon-lined stainless steel vessel, heated to 170 °C for 3 days, followed by slow cooling (a descent rate of 10 °C/h) to room temperature. Green block crystals of **6** were obtained. Yield of 54% (based on Ni). Anal. (%) calcd. for $C_{39}H_{35}NiN_5O_7$: C, 62.92; H, 4.74; N, 9.41. Found: C, 62.73; H, 4.90; N, 9.33. IR (KBr pellet, cm^{-1}): 3440 (s), 3089 (m), 2375 (m), 1667 (s), 1573 (vs), 1434 (vs), 1387 (vs), 1241 (m), 1075 (s), 837 (s), 776 (s), 534 (w).

Synthesis of $[Co(bcpb)(4,4'\text{-bimbp})]_n$ (7). A mixture of H_2bcpb (0.20 mmol, 0.064 g), 4,4′-bimbp (0.20 mmol, 0.053 g), cobalt(II) nitrate hexahydrate (0.20 mmol, 0.058 g), NaOH (0.30 mmol, 0.012 g), and 12 mL H_2O was placed in a Teflon-lined stainless steel vessel, heated to 170 °C for 3 days, followed by slow cooling (a descent rate of 10 °C/h) to room temperature. Red block crystals of **7** were obtained. Yield of 69% (based on Co). Anal. (%) calcd. for $C_{39}H_{29}CoN_5O_4$: C, 67.83; H, 4.23; N, 10.14. Found: C, 66.97; H, 4.54; N, 10.01. IR (KBr pellet, cm^{-1}): 3437 (s), 3067 (m), 2376 (m), 1705 (vs), 1517 (vs), 1412 (vs), 1378 (vs), 1274 (s), 1123 (s), 1017 (s), 836 (m), 762 (s), 544 (w).

Synthesis of $[Mn(pip)(MeOH)(H_2O)]_n$ (8). A mixture of H_2pip (0.20 mmol, 0.031 g), 4,4′-bimbp (0.20 mmol, 0.053 g), manganous(II) sulfate monohydrate (0.20 mmol, 0.340 g), NaOH (0.10 mmol, 0.004 g), 12 mL H_2O was placed in a Teflon-lined stainless steel vessel, heated to 170 °C for 3 days, followed by slow cooling (a descent rate of 10 °C/h) to room temperature. Colorless block crystals of **8** were obtained. Yield of 73% (based on Mn). Anal. (%) calcd. for $C_{33}H_{33}CuN_5O_8$: C, 57.34; H, 4.81; N, 10.13. Found: C, 57.21; H, 5.12; N, 9.79. IR (KBr pellet, cm^{-1}): 3426 (s), 2373 (m), 1605 (vs), 1571 (vs), 1498 (s), 1383 (vs), 1253 (s), 1061 (s), 831 (s), 774 (s), 542 (w).

Synthesis of $\{[Ni(pip)(4,4'\text{-bibp})_{0.5}(H_2O)]\cdot 2H_2O\}_n$ (9). A mixture of H_2pip (0.20 mmol, 0.031 g), 4,4′-bibp (0.20 mmol, 0.057 g), nickel(II) dichloride hexahydrate (0.20 mmol, 0.048 g), NaOH (0.30 mmol, 0.012 g), and 12 mL H_2O was placed in a Teflon-lined stainless steel vessel, heated to 170 °C for 3 days, followed by slow cooling (a descent rate of 10 °C/h) to room temperature. Green block crystals of **9** were obtained. Yield of 61% (based on Ni). Anal. (%) calcd. for $C_{22}H_{19}N_3NiO_7$: C, 53.26; H, 3.86; N, 8.47. Found: C, 53.12; H, 4.17; N, 8.29. IR (KBr pellet, cm^{-1}): 3407 (s), 3120 (m), 2369 (m), 1618 (vs), 1547 (vs), 1438 (vs), 1389 (vs), 1243 (m), 1075 (s), 837 (s), 769 (s), 542 (w).

Synthesis of $\{[Cu(pip)(4,4'\text{-bimbp})]\cdot 4H_2O\}_n$ (10). A mixture of H_2pip (0.20 mmol, 0.031 g), 4,4′-bimbp (0.20 mmol, 0.053 g), copper(II) sulfate pentahydrate (0.20 mmol, 0.050 g), NaOH (0.10 mmol, 0.004 g), and 12 mL H_2O was placed in a Teflon-lined stainless steel vessel, heated to 170 °C for 3 days, followed by slow cooling (a descent rate of 10 °C/h) to room temperature. Blue block crystals of **10** were obtained. Yield of 49 % (based on Cu). Anal. (%) calcd. for $C_{33}H_{33}CuN_5O_8$: C, 57.34; H, 4.81; N, 10.13. Found: C, 57.07; H, 4.73; N, 10.02. IR (KBr pellet, cm^{-1}): 3437 (s), 3067 (m), 2376 (m), 1618 (vs), 1546 (vs), 1442 (vs), 1393 (vs), 1243 (m), 1077 (s), 839 (s), 768 (s), 544 (w).

X-ray crystallography. Intensity data collection was carried out on a Siemens SMART diffractometer equipped with a CCD detector using Mo-*Kα* monochromatized radiation (λ = 0.71073 Å) at 293(2) or 296(2) K. The absorption correction was based on multiple and symmetry-equivalent reflections in the data set using the SADABS program based on the method of Blessing. The structures were solved by direct methods and refined by full-matrix least-squares using the SHELXTL package.[14] Crystallographic data for complexes **1**–**10** are given in Table 1. Selected bond lengths and angles for **1**–**10** are listed in Table S1. For complexes of **1**–**10**, further details on the crystal structure investigations may be obtained from the Cambridge Crystallographic Data Centre, CCDC, 12 Union Road, CAMBRIDGE CB2 1EZ, UK, [Telephone:+44-(0)1223-762-910, Fax: +44-(0)1223-336-033; E-mail: deposit@ccdc.cam.ac.uk, http://www.ccdc.cam.ac.uk/deposit], on quoting the depository number CCDC-932484 for **1**, 9932487 for **2**, 932489 for **3**, 932486 for **4**, 932488 for **5**, 932490 for **6**, 932485 for **7**, 949697 for **8**, 949698 for **9**, and 949699 for **10**. Topological analysis of the coordination networks of all the compounds was performed with the program package TOPOS.[15]

Result and discussion

Synthesis and Characterization. In the present study, complexes **1-10** were prepared from the solvothermal reaction of the related first transitional metal salts and the trifunctional pyridine-dicarboxylate (H_2pip, H_2bcpb) in the presence of rigid or flexible (bis)imidazole bridging linkers (1,4-bmib, 4,4'-bibp, and 4,4'-bimbp). All the complexes **1-10** are stable in the solid state upon extended exposure to air. They have poor solubility in water and common organic solvents, but can be slightly soluble in very high polarity solvents.

The Structural Comparison and Discussion. As shown in the Scheme 2, both of H_2bcpb and H_2pip are completely deprotonated and adapted similar coordination modes to link three M^{II} ions *via* the pyridyl N atoms and two μ_1 carboxyl groups. It is also worth noting that the coordination modes of $bcpb^{2-}$ and pip^{2-} varied in the presence of different (bis)imidazole ancillary ligands. The pyridyl N atoms coordinated with metal ions (Co^{II}, Ni^{II}, Mn^{II}) in all the complexes. As for $bcpb^{2-}$, both of two carboxyl groups adopt η^1:η^1 coordination modes in complexes **1-3** (named as Mode I, shown in Scheme 2), η^1 in **4-6** (Mode II), and η^1:η^1 and η^1 (Mode III) in **7**. Two carboxyl groups of pip^{2-} show three different coordination modes in three complexes, η^1:η^1 (Mode IV) in **8**, η^1:η^1 and η^1 (Mode V) in **9**, andη^1 (Mode VI) in **10**. Thus, the various coordination modes of carboxylate groups resulted in ten coordination polymers with seven different topologies. The various frameworks could be

mainly attributed to the "synergistic reaction" of the length (l_p) and width (l_c) from the organic skeletons including the trifunctional pyridine-dicarboxylate (H_2pip, H_2bapb) and (bis)imidazole bridging linkers (1,4-bmib, 4,4'-bibp, and 4,4'-bimbp). For example, for compounds **1**, **4**, and **7**, although the similar environments are employed except for three different (bis)imidazole bridging linkers (1,4-bmib, 4,4'-bibp, 4,4'-bimbp), their related architectures exhibit (3,5)-connected $(6^2\cdot8)(6^3\cdot8\cdot10^2)$, (3,4)-connected $(4\cdot7^2)(4\cdot7^5\cdot8^4)$, and 2-fold (3,5)-connected $(6^3)(6^9\cdot8)$ 3D topologies, respectively. The different topologies could be attributed to the distances (*trans*- or *cis*-) and distorted angles between two coordinated nitrogen atoms in (bis)imidazole bridging linkers.

In a word, not only the length (l_p) and width (l_c) of the trifunctional pyridine-dicarboxylate ligands but also the flexible and length of the (bis)imidazole bridging linkers have great effect on the final packing structures.

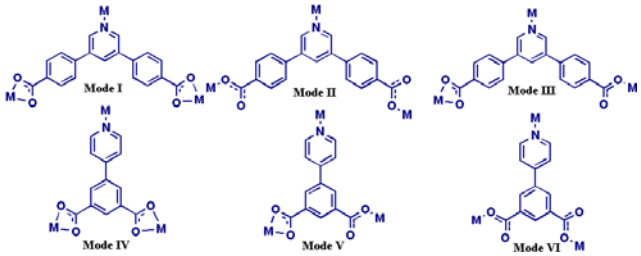

Scheme 2. The coordination modes of pip2-, bcpb2- in complexes **1**-**10**.

Table 1 Crystal data for **1 – 10**

Compound	**1**	**2**	**3**	**4**	**5**
Empirical formula	$C_{54}H_{42}Co_2N_6O_9$	$C_{27}H_{20}CuN_3O_4$	$C_{27}H_{20}N_3NiO_4$	$C_{56}H_{48}Co_2N_6O_{14}$	$C_{28}H_{20}CuN_3O_5$
Formula weight	1036.80	514.00	509.17	1146.86	542.01
Crystal system	Monoclinic	Monoclinic	Monoclinic	Monoclinic	Monoclinic
Space group	*C2/c*	*C2/c*	*C2/c*	*C2/c*	*C2/c*
a (Å)	20.201(1)	20.307(9)	20.249(1)	27.381(5)	26.386(2)
b (Å)	9.992(7)	10.191(0)	10.011(5)	11.289(2)	11.395(7)
c (Å)	21.796(2)	21.846(1)	22.164(1)	18.020(4)	17.566(7)
α (°)	90.00	90.00	90.00	90.00	90.00
β (°)	91.23(4)	91.20(1)	91.22(8)	117.07(5)	115.71(2)
γ (°)	90.00	90.00	90.00	90.00	90.00
V(Å^3)	4399(5)	4520(2)	4492(4)	4959(6)	4759(2)
Z	4	8	8	4	8
D_{calcd} (Mg/m^3)	1.566	1.511	1.506	1.536	1.513
μ(mm^{-1})	0.825	1.007	0.905	0.747	0.964
θ range (°)	1.78–25.00	1.86–25.00	1.84–28.35	1.67–28.28	1.71–25.00
Reflections collected/	10535	11447	14010	15561	12024
Unique reflection	3867	3991	5483	6136	4185
Data/Parameters	3867/326	3991/317	5483/317	6136/360	4185/340
F(000)	2136	2112	2104	2368	2224
T(K)	293(2)	293(2)	296(2)	293(2)	296(2)
R_{int}	0.0535	0.0546	0.0793	0.0696	0.0804
R_1 (wR_2) [$I > 2\sigma(I)$]	0.0472 (0.1163)	0.0537 (0.1399)	0.0572 (0.1034)	0.0572 (0.1268)	0.0634 (0.1649)
R_1 (wR_2) (all data)	0.0757 (0.1359)	0.0842 (0.1619)	0.1267 (0.1259)	0.0847 (0.1479)	0.1123 (0.1987)
Gof	0.997	1.001	1.002	0.999	0.999
Compound	**6**	**7**	**8**	**9**	**10**
Empirical formula	$C_{78}H_{72}Ni_2N_{10}O_{15}$	$C_{39}H_{29}CoN_5O_4$	$C_{14}H_{12}MnNO_6$	$C_{22}H_{20}NiN_3O_7$	$C_{33}H_{33}CuN_5O_8$
Formula weight	1506.88	690.60	345.19	497.12	591.18
Crystal system	Monoclinic	Triclinic	Monoclinic	Monoclinic	Triclinic
Space group	*C*2/*c*	*P-1*	*Cc*	*C*2/*c*	*P*-1
a (Å)	32.498(8)	11.691(7)	20.768(5)	17.241(6)	16.8210(12)
b (Å)	12.812(3)	11.788(2)	10.017(3)	15.950(6)	19.1858(14)
c (Å)	18.172(5)	12.651(1)	16.158(4)	16.740(6)	20.6555(15)
α (°)	90	82.07(1)	90	90	90
β (°)	94.661(5)	83.11(3)	121.098(4)	108.386(7)	90
γ (°)	90	82.63(8)	90	90	90
V(Å^3)	7541(3)	1703(4)	2878(3)	4368(3)	6666(1)
Z	4	2	8	8	8
D_{calcd} (Mg/m^3)	1.327	1.346	1.593	1.512	1.377
μ(mm^{-1})	0.571	0.552	0.946	0.938	0.713
θ range	1.71–25.00	1.76–25.00	2.29–25.00	1.78–28.22	1.89–25.00
Reflections collected	17912	8848	7094	13599	32497
Unique reflection	6577	5952	2538	5255	5870
Data/Parameters	6577/470	5952/442	2538/203	5255/298	5870/448
F(000)	3096	714	464	2700	2872
T(K)	293(2)	293(2)	293(2)	296(2)	293(2)
R_{int}	0.0649	0.0161	0.0184	0.0943	0.1541
R_1 (wR_2) [$I > 2\sigma(I)$]	0.0784 (0.2194)	0.0487 (0.1409)	0.0538 (0.1850)	0.0673 (0.1448)	0.0658 (0.1512)
R_1 (wR_2) (all data)	0.1293 (0.2617)	0.0609 (0.1518)	0.0598 (0.1914)	0.1541(0.1829)	0.1506 (0.1747)
Gof	1.006	1.003	0.999	0.997	1.002

$R_1 = \Sigma| |F_o|-|F_c| | / \Sigma|F_o|$, $wR_2 = [\Sigma w(F_o^2-F_c^2)^2]/ \Sigma w(F_o^2)^2]^{1/2}$

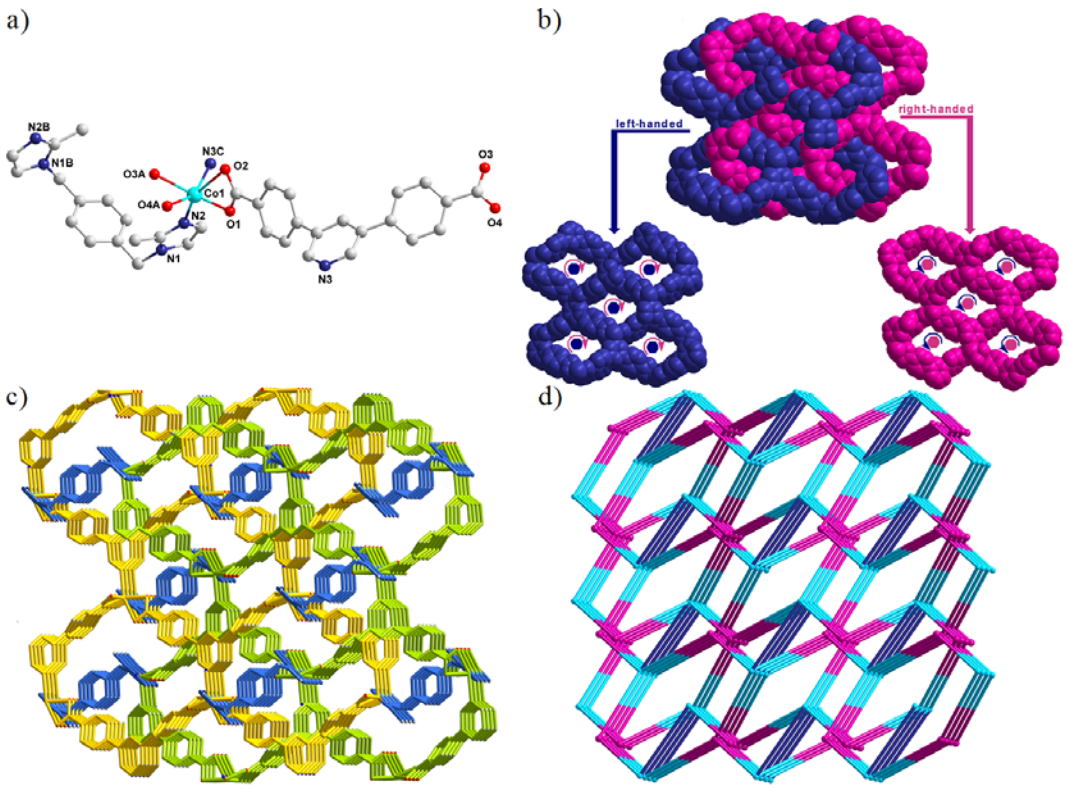

Figure 1. (a) Coordination environment of Co^{II} ion in **1** (Symmetry codes: A: 0.5+*x*, -0.5-*y*, 0.5+*z*; B: 2-*x*, *y*, 1.5-*z*; C: 0.5+*x*, 0.5+*y*, *z*). (b) Two penetrated chiral **ths** networks. (c) The 3D frameworks with 3-connected nets. (d) Schematic view of a (3,4)-connected **amd** topology with the Schläfli symbol of $(6^2{\cdot}8)(6^3{\cdot}8{\cdot}10^2)$ of **1** (green spheres: Co^{II} atoms; violet spheres: $bcpb^{2-}$ ligands; blue bonds: 1,4-bmib ligands).

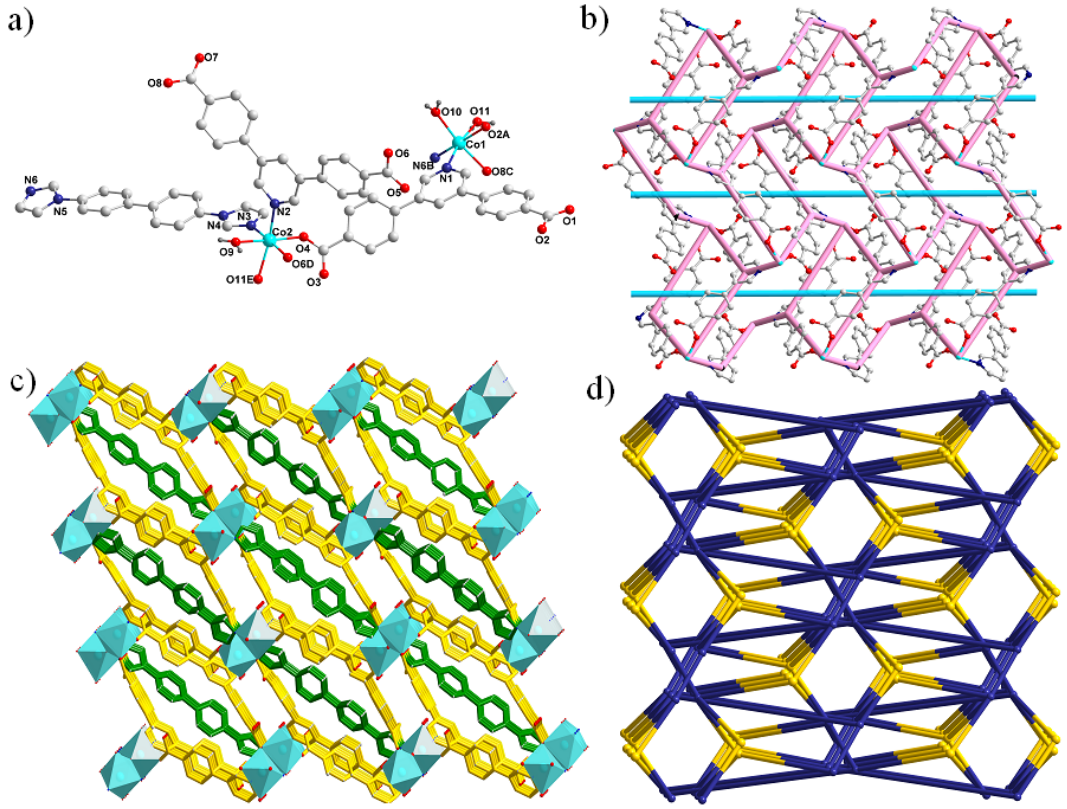

Figure 2. (a) Coordination environment of Co^{II} ion in **4** (Symmetry codes: A: –0.5–*x*, 1.5–*y*, –1-*z*; B: 0.5–*x*, 1.5–*y*, 1–*z*; C: 0.5–*x*, 0.5+*y*, 0.5–*z*.). (b) View of the 3-connected 2D network. (c) The (3,5)-connected 3D frameworks of **4**. (d) Schematic view of the (3,5)-connected $(4{\cdot}7^2)(4{\cdot}7^5{\cdot}8^4)$ network of **4** (dark blue spheres: Co^{II} atoms; yellow spheres: $bcpb^{2-}$ ligands; dark blue bonds: 4,4′-bibp ligands).

Structural Description of {[M(bcpb)(1,4-bmib)$_{0.5}$]·xH_2O}$_n$ (M = Co (1), Cu (2), Ni (3), x= 1 for 1, 0 for 2 and 3). Single-crystal X-ray diffraction analysis revealed that complexes **1-3** are isomorphic and crystallize in the monoclinic system, space group *C2/c*. Herein only the structure of **1** will be discussed as a representation. As shown in Figure 1a, there is one crystallographically independent Co^{II} atom, one $bcpb^{2-}$ ligand, half a 1,4-bmib ligand, and one lattice water molecule in the asymmetric unit. Each Co^{II} centre is hexa-coordinated by: two N atoms from one 1,4-bmib ligand and one $bcpb^{2-}$ ligand [Co(1)–N(2) = 2.037(6), Co(1)–N(3) = 2.075(6) Å], and four O atoms from three two $bcpb^{2-}$ ligands [Co(1)–O(1) = 1.970(8), 25 Co(1)–O(2) = 2.589(5), Co(1)–O(3) = 2.110(2), Co(1)–O(4) = 2.158(7) Å], showing a distorted octahedral coordination geometry. Both Co–N and Co–O bond lengths are well-matched to the similar complexes.[16]

The ligand of H_2bcpb is completely deprotonated and acts as one μ_3 node to coordinate with three Co^{II} ions via three dentate atoms including one N and two O atoms, in which both of two carboxyl groups adopt similar η^1:η^1 coordination mode (named as Mode **I**, Scheme 2).The dihedral angles between the two phenyl rings and the pyridine ring in $bcpb^{2-}$ are 33.22(2) and 54.24(2)°, respectively. And the one between the two phenyl rings in $bcpb^{2-}$ is 44.92(1)°. It is worth noting that the dihedral angles are much larger for compounds **2** and **3**: 34.20(1), 54.33(1), and 44.18(1) for **2**; 33.22(1), 55.75(1), and 46.77(1)° for **3**. The divalent Co^{II} ions are linked by 3-connected $bcpb^{2-}$ ligands to form two interpenetrated double-layers with the alternately arranged left- and right-handed helical chains, which are further linked by the 1,4-bmib ligands to generate a polymeric **ths** 3D [Co(bcpb)]$_n$ network with the 11.621(6) × 11.268(5) $Å^2$ opening 1D channels (Figure 1b). The two kinds of chiral 3D networks are further bridged by 1,4-bimb ligands to result in an achiral self-catenation frameworks (Figure 1c).

The topological analysis method was accessed to simplify the structure. The overall framework can be defined as a (3,4)-connected 3D **amd** network, with the Point Schläfli symbol of $(6^2·8)(6^3·8·10^2)$ by denoting the Co^{II} and $bcpb^{2-}$ as four-connected and three-connected nodes, respectively (Figure 1d).

Structural Description of {[Co(bcpb)(4,4'-bibp)$_{0.5}$(H_2O)$_{1.5}$]·1.5H_2O}$_n$ (4). Although the compounds **4** and **5** are constructed from the same organic ligands in the similar reaction environments, they exhibit different 3D architectures due to completely different coordination geometry: (3,5)-connected (3,5)-connected $(4·7^2)(4·7^5·8^4)$ topology for **4** and 2-fold (3,4)-connected $(4·8^2)(4·8^5)$ **dmc** for **5**. Complex **4** crystallizes in the monoclinic space group *C2/c*. The asymmetric unit contains one crystallographically independent Co^{II} atoms, one $bcpb^{2-}$ ligands, a half of 4,4'-bibp ligands, one and a half associated water molecules, and one and a half of lattice water molecules (Figure 2a). The Co^{II} cation is coordinated with four oxygen atoms from two different $bcpb^{2-}$ ligands, one μ_1- and one μ_2- coordinated water molecules, and two nitrogen atoms from two 4,4'-bibp ligands, leaving a distorted octahedral geometry with {CoN_2O_4} coordination environments. The bond lengths of Co-O are in the range of 2.066(7)-2.149(5) Å, and the Co-N are 2.089(7), 2.145(8) Å, respectively.

Slightly different from that in **1-3**, two carboxyl groups of $bcpb^{2-}$ in **4-6** adopts η^1 coordination mode (Mode **II**). The dihedral angle between two phenyl rings and central pyridine ring in $bcpb^{2-}$ are 16.08(1)/20.16(1) and 40.05(1)/40.49(1)°, respectively. And the one between two phenyl rings in one $bcpb^{2-}$ is 49.97(1)/54.52(1)°. Co^{II} cations are linked by $bcpb^{2-}$ to form 2D 3-connected [Co(bcpb)]$_n$ networks with the right- and left-handed helix alternating (Figure 2b), which are bridged by μ_2-H_2O to generate a 3D framework with 1D channels. Furthermore, metal ions are linked by 4,4'-bibp ligands along the channels to exhibit an unprecedented (3,5)-connected networks with the Schläfli symbol of $(4·7^2)(4·7^5·8^4)$ by denoting the Co^{II} atoms to five-connected nodes and $bcpb^{2-}$ ligands to three-connected nodes, respectively (Figure 2c and Figure 2d).

Structural Description of [Cu(bcpb)(4,4'-bibp)$_{0.5}$(H_2O)]$_n$ (5). Single-crystal X-ray diffraction analysis reveals that complex **5** crystallizes in the monoclinic system, space group *C2/c*. As shown in Figure 3a, there are one crystallographically independent Cu^{II} atom, one $bcpb^{2-}$ ligand, a half of 4,4'-bibp ligand, and one associated water molecular in the asymmetric unit. Each Cu^{II} centre is penta-coordinated by two N atoms from one 4,4'-bibp ligand and one $bcpb^{2-}$ ligand [Cu(1)–N(1) = 2.320(1) and Cu(1)–N(2) = 1.988(5) Å], and three O atoms from two another $bcpb^{2-}$ ligands and one coordinated water molecule [Cu(1)–O(1) = 1.938(2), Cu(1)–O(4) = 1.975(4), and Cu(1)–O(5) = 1.968(1) Å], showing a distorted tetragonal pyramid coordination geometry.

The ligand of $bcpb^{2-}$ acts as one μ_3 node to coordinate with three Cu^{II} ions *via* the deprotonated carboxylate oxygen atom and the N atom (Mode **II**). The dihedral angle between two phenyl rings and central pyridine ring in $bcpb^{2-}$ are 22.38(1) and 39.66°, respectively. And the one between two phenyl rings in one $bcpb^{2-}$ is 55.49°. The 3-connected $bcpb^{2-}$ ligands connect Co^{II} cations to form 2D double-layer networks with right- and left-helix chains alternately arrange (Figure 3b). Furthermore, the 4,4'-bibp ligands act as pillars to link the neutral layers into a 3D framework (Figure 3c). The Co···Co distance separated by the 4,4'-bibp ligand is 17.768(7) Å.

At the sight of topology, the whole structure of complex **5** can be defined as a 2-fold (3,4)-connected **dmc** network with the Schläfli symbol of $(4·8^2)(4·8^5)$ by denoting the Cu^{II} atoms to four-connected nodes and $bcpb^{2-}$ ligands to three-connected nodes, respectively (Figure 3d).

Structural Description of {[Ni(bcpb)(4,4'-bimbp)(H_2O)]·2.5H_2O}$_n$ (6). X-ray diffraction analysis reveals that complex **6** crystallizes in the monoclinic *C2/c* space group. As shown in Figure 4a, there are one crystallographically independent Ni^{II} atom, one $bcpb^{2-}$ ligand, one 4,4'-bimbp ligand, and one coordinated water molecules, and two and a half of lattice water molecules in the asymmetric unit. Each Ni^{II} centre is penta-coordinated by three N atoms from two different 4,4'-bimbp ligands and one $bcpb^{2-}$ ligand [Ni(1)–N(1) = 2.091(3), Ni(1)–N(4) = 2.063(6), and Ni(1)–N(5) = 2.114(5) Å], and three O atoms from another two $bcpb^{2-}$ ligands and one associated water molecule [Ni(1)–O(1) = 2.068(8), Ni(1)–O(2) = 2.088(5), and Ni(1)–O(1W) = 2.078(9) Å], showing a distorted tetragonal pyramid coordination geometry.

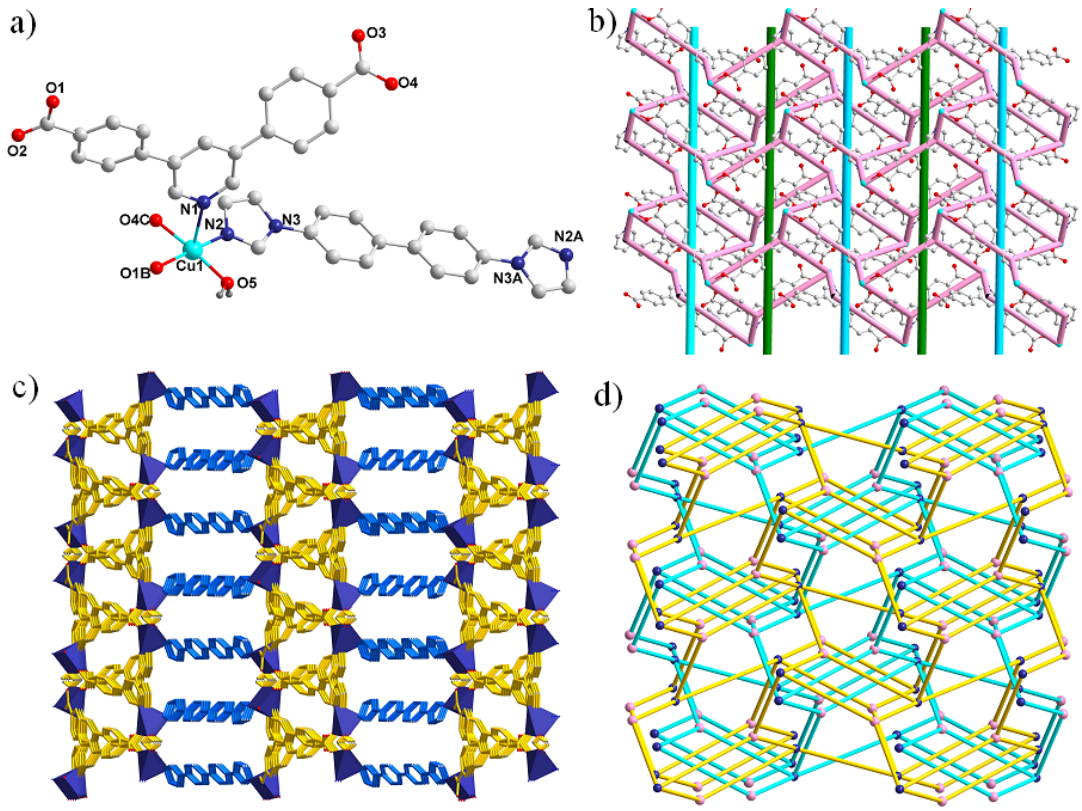

Figure 3. (a) Coordination environment of Cu^{II} ion in **5** (Symmetry codes: A: -0.5–*x*, 1.5-*y*, -*z*; B: 0.5-*x*, -0.5+*y*, 1.5-*z*; C: *x*, 2-*y*, 0.5+*z*). (b) The 2D $[Cu(bcpb)]_n$ net constructed by $bcpb^{2-}$ ligands linked with Cu^{II} cations. (c) View of the (3,4)-connected 3D frameworks of **5** (purple pheres: Cu^{II} atoms; yellow spheres: $bcpb^{2-}$ ligands; blue spheres: 4,4'-bibp ligands). (d) Schematic view of the 2-fold (3,4)-connected **dmc** network of **5** (dark blue spheres: Cu^{II} atoms; pink spheres: $bcpb^{2-}$ ligands).

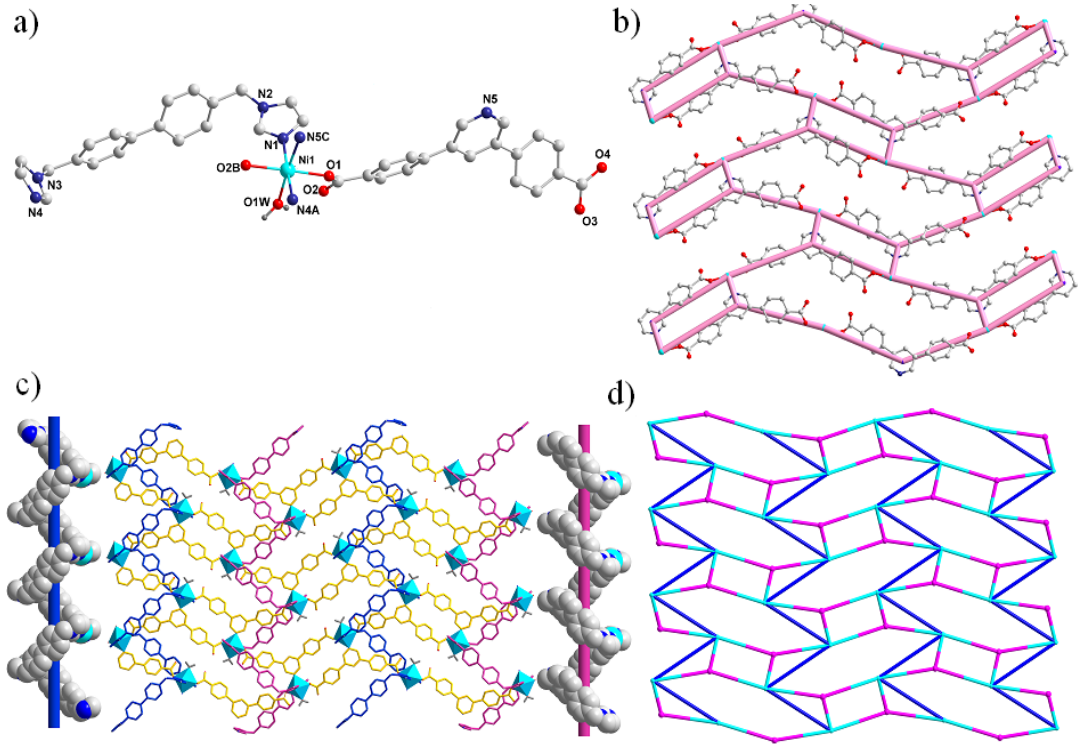

Figure 4. (a) Coordination environment of Ni^{II} ion in **6** (Symmetry codes: A: 0.5–*x*, -0.5+*y*, 0.5-*z*; B: -0.5+*x*, 1.5-*y*, -0.5+*z*; C: 1-*x*, 1-*y*, -*z*). (b) The 2D 3-connected net constructed by the $bcpb^{2-}$ ligands linked Ni^{II} ions. (c) View of the right- and left-handed helix chains modified 2D $[Ni(bcpb)]_n$ networks. (d) Schematic view of the (3,5)-connected **gek1** networks of **6** (green spheres: Ni^{II} atoms; violet spheres: $bcpb^{2-}$ ligands; blue bonds: 4,4'-bimbp ligands).

The dihedral angle between two phenyl rings and central pyridine ring in bcpb^{2-} are 27.56(1) and 27.80(1)°, respectively. And the one between two phenyl rings in one bcpb^{2-} is 53.86(1)°. The 3-connected bcpb^{2-} ligands connect Ni^{II} cations to form 2D [Ni(bcpb)]$_n$ networks (Figure 4b), which are further intra-linked by 4,4'-bibp ligands along *b* direction. It is noteworthy that the [Ni(4,4'-bibp)]$_n$ chains show right- and left-handed helixes with the Ni···Ni distance separated by the 4,4'-bimbp ligand being 12.136(6) Å (Figure 4c).

Topological analysis shows the whole structure of complex **6** can be defined as a (3,5)-connected 2D **gek1** network with the Schläfli symbol of $(4\cdot8^2)(4\cdot8^5)$ by denoting the Ni^{II} atoms to five-connected nodes and bcpb^{2-} ligands to three-connected nodes, respectively (Figure 4d).

Structural Description of [Co(bcpb)(4,4'-bimbp)]$_n$ (7). Complex **4** was obtained as a 2-fold interpenetrated 3,5-coordinated 3D network with a **gra** topology. It crystallized in triclinic *P-1* space group. As shown in Figure 5a, there are one crystallographically independent Co^{II} atom, one bcpb^{2-} ligand, and one 4,4'-bimbp ligand in the asymmetric unit. Each Co^{II} centre is hexa-coordinated by three N atoms from two 4,4'-bibp ligands and one bcpb^{2-} ligand, and three O atoms from two bcpb^{2-} ligands, showing a distorted octahedral coordination geometry. The Co–N/O bond distances are range from 2.018(6) to 2.267(5) Å, similar with the reported ones.

The two carboxylate groups of bcpb^{2-}, different from the ones in **1-6**, adopt η^1:η^1 and η^1 coordination modes (Mode **III**). The dihedral angles between two phenyl rings and central pyridine ring in bcpb^{2-} are 24.25(1) and 30.11(1)°, respectively. And the one between two phenyl rings is in bcpb^{2-} is 17.60°. It is worth noting that the dihedral angles are much smaller than the ones in **1-6**, which may be attributed to the interpenetrating of the whole structure. The Co(II) ions are bridged by bcpb^{2-} ligands to result in a 2D networks (Figure 5b), which are further extended *via* the bridge of 4,4'-bimbp to form a corrugated 3D framework with 1D channels, leaving the 11.691(6) × 18.696(2) Å^2 pores along *b* axis (Figure 5c). Moreover, adjacent nets are further interpenetrated with each other to result in a 2-fold 3D interpenetrating frameworks.

The topology analysis shows the overall framework of complex **7** can be rationalized to a (3,5)-connected **gra** topology with the Schläfli symbol of $(6^3)(6^9\cdot8)$ by denoting the Co^{II} atoms to five-connected nodes and bcpb^{2-} ligands to three-connected nodes, respectively (Figure 5d).

Structural Description of [Mn(pip)(MeOH)(H$_2$O)]$_n$ (8). Structural analysis indicates that complex **8** crystallizes in the monoclinic *C2/c* space group. The asymmetric unit of **8** is composed of one crystallographically independent Mn^{II} atom, one pip^{2-} ligand, one methanol molecule, and one free water molecule. The coordination environment around the Mn(II) atom is exhibited in Figure 6a. Each Mn^{II} ion is located in a slightly {MnNO$_6$} distorted pentagonal bipyramid geometry, completed by one N atoms belonging to one pip^{2-} ligand and six O atoms from another two pip^{2-} ligands, one MeOH molecule, and one coordinated water molecule. The Mn–N/O bond lengths span in the range of 2.186(3)–2.629(1) Å.

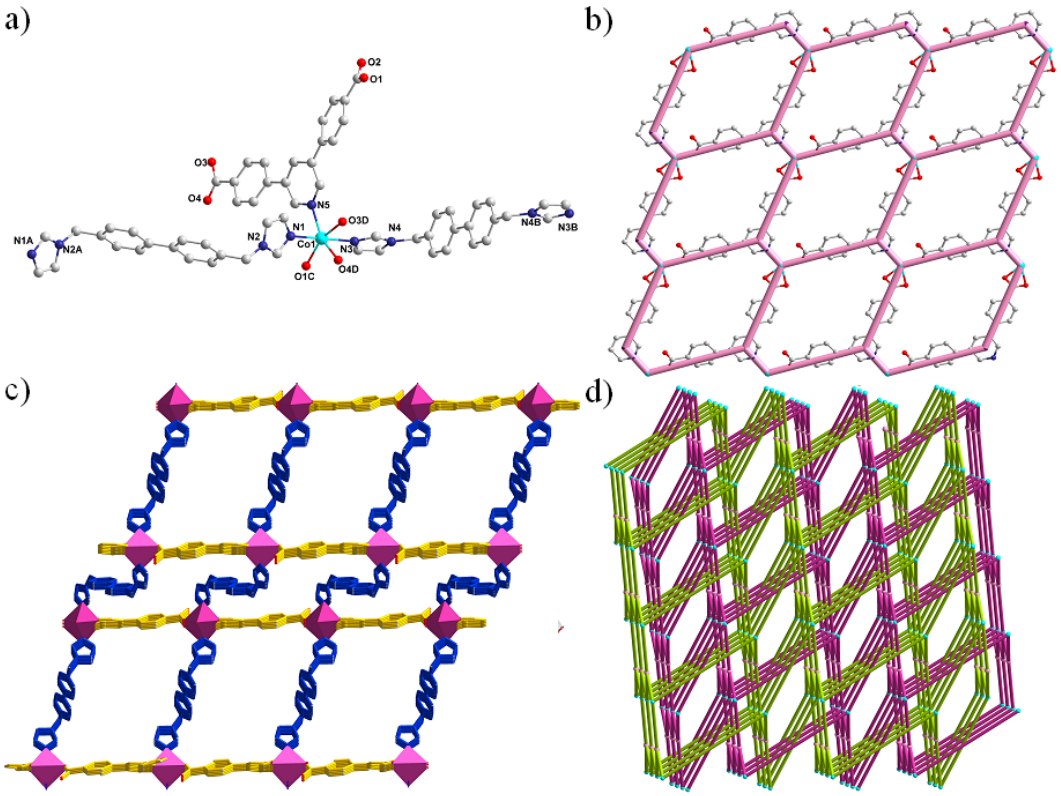

Figure 5. (a) Coordination environment of Co^{II} ion in **7** (Symmetry codes: A: 2–*x*, 2-*y*, -*z*; B: 1-*x*, -*y*, 2-*z*; C: 1+*x*, *y*, *z*; D: *x*, -1+*y*, *z*.). (b) The 2D 6^3-**hcb** net constructed from the bcpb^{2-} ligands connected the Co^{II} ions. (c) The 3D frameworks constructed with the 4,4′-bimbp linked the 2D 6^3-**hcb** nets. (d) Schematic view of the (3,5)-connected **gra** network of **7** (green spheres: Co^{II} atoms; pink spheres: bcpb^{2-} ligands).

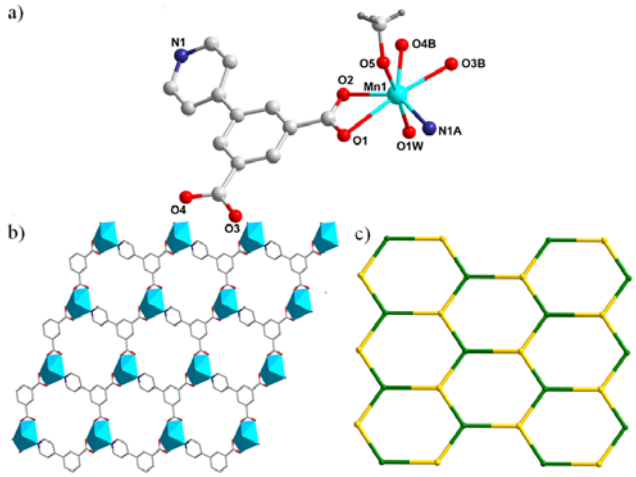

Figure 6. (a) Coordination environment of Mn^{II} ion in **8** (Symmetry codes: A: 0.5+*x*, 0.5+*y*, *z*; B: *x*, 1+*y*, *z*). (b) The 2D $[Mn(pip)]_n$ nets constructed form pip^{2-} ligands and Mn^{II} ions. (c) Schematic view of the 3-connected 6^3-**hcb** network (grass green spheres: Mn^{II} atoms; yellow spheres: pip^{2-} ligands).

The ligand of H_2pip is completely deprotonated and act as one μ_3 node to coordinate with three Mn^{II} ions, in which two carboxyl groups adopt η^1 and η^1:η^1 coordination modes (Mode **IV**). The dihedral angles between phenyl ring and central pyridine ring in pip^{2-} is 5.16(1)°, and all non-hydrogen atoms of pip^{2-} are nearly located in one planar. MeOH and associated H_2O molecules occupied the axial sites of the pentagonal bipyramid coordination geometry. Thus this acts as an impetus to generate a 2D polymeric $[Mn(pip)]_n$ layer rather than a 3D framework, shown in Figure 6b. The closest through-ligand Mn···Mn distances along *a* and *b* axi are 10.017 and 11.528 Å, respectively.

From the viewpoint of structural topology, the overall framework of **8** can be defined as a 3-connected 6^3-**hcb** topology by denoting both Mn^{II} and $bcpb^{2-}$ as three-connected nodes, respectively (Figure 6c).

Structural Description of $\{[Ni(pip)(4,4'\text{-bibp})_{0.5}(H_2O)]\cdot 2H_2O\}_n$ (9). Single-crystal X-ray diffraction analysis reveals that complex **9** crystallizes in the monoclinic system, space group *C2/c*. As shown in Figure 7a, there are one crystallographically independent Ni^{II} atom, one pip^{2-} ligand, a half of 4,4'-bimbp ligand, and one associated and two lattice water molecules in the asymmetric unit. Each Ni^{II} center is hexa-coordinated by two N atoms from one 4,4'-bibp ligand and one pip^{2-} ligand [Ni(1)–N(2) = 2.073(8), and Ni(1)–N(1) = 2.070(3) Å], and four O atoms from two pip^{2-} ligands and one associated water molecule [Ni(1)–O(1) = 2.016(4), Ni(1)–O(5) = 2.087(0) , Ni(1)–O(3) = 2.100(8) and Ni(1)–O(4) = 2.190(8) Å].

The ligand of H_2pip is completely deprotonated and acts as one μ_3 node to coordinate with three Ni^{II} ions, in which two carboxyl groups adopt η^1:η^1 and η^1 coordination mode (Mode **V**). The dihedral angle between the phenyl ring and pyridine ring in pip^{2-} is 5.87(1). The Ni^{II} ions were connected by the pip^{2-} ligands to form two 3D porous frameworks with the effective sizes of the channels being 11.74 × 11.74 $Å^2$ (Figure 7b). The two kinds of 3D networks are further bridged by 4,4'-bimbp ancillary ligands to result in an interpenetrated unusual framework (Figure 7c).

To better insight of the complicated 3D architecture, topology analysis was introduced. This 3D net exhibits an interesting self-catenation phenomenon, but most important is that it can be easily decomposed to two interpenetrating 3D nets by breaking just the two Ni1-N2 bonds. Each of the decomposed nets can be described as 3-coordinated 10^3-**srs** net. The overall structure of **9** can be regard as a (3,4)-connected 3D framework with point Schläfli symbol of $(6^2\cdot 8)(6^3\cdot 8\cdot 10^2)$ (Figure 7d).

Structural Description of $\{[Cu(pip)(4,4'\text{-bimbp})]\cdot 4H_2O\}_n$ (10). X-ray diffraction analysis reveals that complex **10** is an unprecedented (3,5)-connected 3D framework. It crystallizes in the orthorhombic with space group of *Pbca*. The asymmetric unit consists of one Cu^{II} atom, one pip^{2-}, one 4,4'-bimbp, and four free water molecules. As depicted in Figure 8a, each Cu^{II} center is coordinated by three N atoms from one pip^{2-} and two 4,4'-bimbp [Cu(1)–N(1) = 1.988(7), Cu(1)–N(4) = 1.997(4), and Cu(1)–N(5) = 2.339(9) Å], and two carboxylic O atoms from two another $bcpb^{2-}$ ligands [Cu(1)–O(4) = 1.961(0), and Cu(1)–O(1) = 1.968(3) Å], displaying a distorted tetragonal pyramid coordination geometry.

The ligand of H_2pip is completely deprotonated and acts as one μ_3 node to coordinate with three Cu^{II} cations, in which two carboxyl groups adopt η^1 coordination mode (Mode **VI**). The dihedral angle between the phenyl ring and pyridine ring in pip^{2-} is 22.83(1). The Cu^{II} ions were connected by the pip^{2-} ligands to form 2D $[Cu(pip)]_n$ layers, between which the unprecedented $[(H_2O)_8(O_{carboxyl})_4]$ water clusters are observed (Figure 8b). Those 2D $[Cu(pip)]_n$ layers are further bridged 4,4'-bimbp ligands to result in a 3D framework (Figure 8c). The interactions between the host frameworks and lattice water molecules are O-H···O hydrogen bonds (O6-H4W···$O2^i$ =2.869 Å, O7-H5W···O3 = 3.011 Å, and O5-H1W···$O3^i$ = 2.806 Å, Symmetry codes: (i) -*x*+1, *y*+1/2, -*z*+3/2), which make the whole structure more stable.

From the topology view, the whole structure of **10** can be regard as a (3,5)-connected $(4\cdot 6\cdot 8)(4\cdot 6^4\cdot 8^5)$ framework by denoting the Cu^{II} ions to five-connected nodes and pip^{2-} ligands to three-connected nodes, respectively (Figure 8d).

IR spectra. The IR spectra of complexes **1**–**10** and H_2bcpb ligand are shown in Figure 9 and Figure S1. For complexes **1**–**7**, **8**–**10,** the similar peaks in the range 1200-1700 cm^{-1} indicated the (bis)imidazole bridging linkers have little effect on the IR characteristic spectra of carboxylate groups. The peaks of those complexes in the range of 1485–1682 cm^{-1} are corresponded with the symmetric and asymmetric stretching the carboxylic groups. The (ν_{as}-ν_s) values (142/130 cm^{-1} for **1**, 167/146 cm^{-1} for **2**, 138/135 cm^{-1} for **3**, 212/185 cm^{-1} for **4**, 180/210 cm^{-1} for **5**, 182/184 cm^{-1} for **6**, 140/193 cm^{-1} for **7**, 128/170 cm^{-1} for **8**, 147/171 cm^{-1} for **9**, and 167/174 cm^{-1} for **10**) are attributed to the diverse carboxylate coordination modes, which are in accordance with the spectroscopic criteria on determining the modes of the carboxylate binding (Δ(chelating) < Δ(bridging) < Δ(monodentate)).[17]

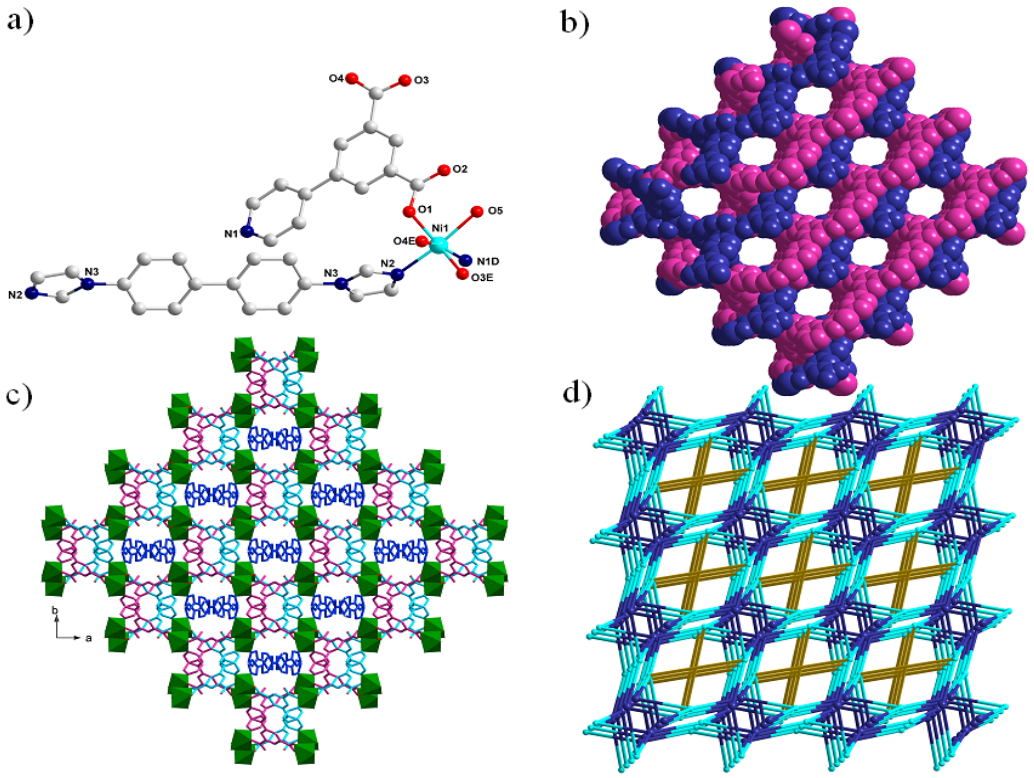

Figure 7. (a) Coordination environment of Ni^{II} ions in **9**. Symmetry codes: (A) *–x*, 1-*y*, 1-*z*; (D) *x*, 1-*y*, -0.5+*z*; (E) -0.5+*x*, 0.5-*y*, -0.5+*z*. (b) The space-filling drawing showing the two $[Ni(pip)]_n$ nets with large channels. (c) View of the 3D frameworks bridged by the 4,4'-bimbp ligands (grass freen spheres: Ni^{II} atoms). (d) Schematic view of the unprecedented (3,5)-connected network of **9** (green spheres: Ni^{II} atoms; dark blue spheres: $bcpb^{2-}$ ligands; brown bonds: 4,4'-bimbp ligands).

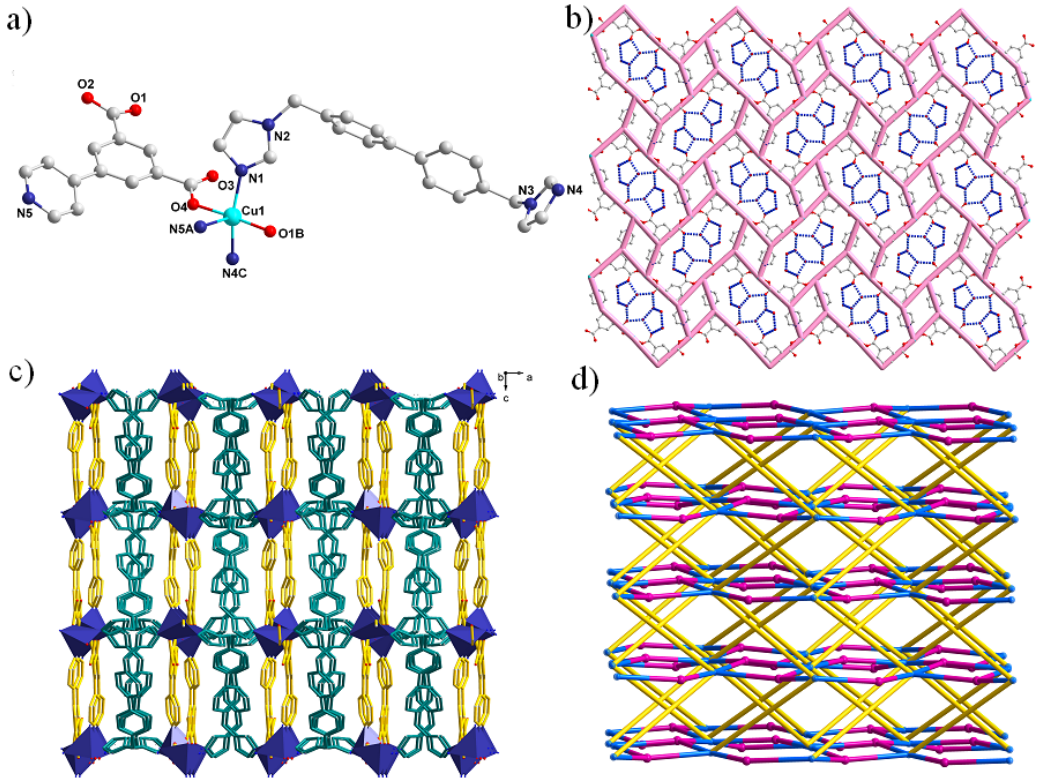

Figure 8. (a) Coordination environment of Cu^{II} ions in **10**. Symmetry codes: (A) 1–*x*, -*y*, 1-*z*; (B) 1-*x*, 0.5+*y*, 1.5-*z*; (C) –0.5+*x*, 0.5-*y*, 2-*z*. (b) The 2D $[Cu(pip)]_n$ networks fulfilled by the unprecedented water cluster $[(H_2O)_8(O_{carboxyl})_4]$. (c) View of the 3D frameworks constructed by the 4,4'-bimbp ligands bridged the $[Cu(pip)]_n$ networks. (d) Schematic view of the (3,5)-connected $(4{\cdot}6{\cdot}8)(4{\cdot}6^4{\cdot}8^5)$ network of **10** (blue spheres: Cu^{II} atoms; pink spheres: pip^{2-} ligands; yellow bonds: 4,4'-bimbp ligands).

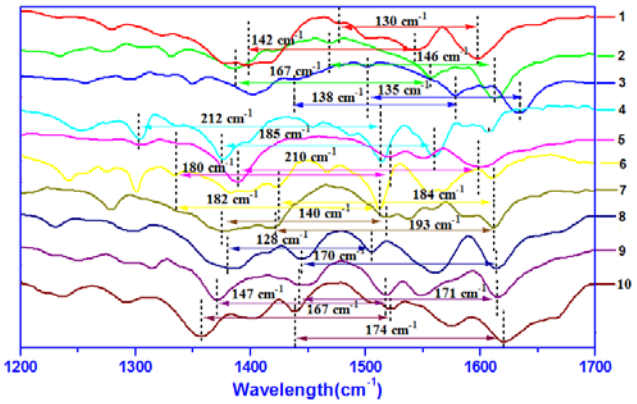

Figure 9. Infrared spectras of **1**-**10**: displaying the positions of the peaks which allow one to characterize the coordination modes in the CPs.

X-ray Power Diffraction Analyses and Thermal Analyses. Powder X-ray diffraction (XRD) has been used to check the phase purity of the bulk samples in the solid state. For complex **1**–**10**, the simulated patterns generated from the results of single-crystal diffraction data with the help of Mercury program,[18] indicative of pure products (Figure S2, Supporting Information).

The thermogravimetric (TG) analysis was performed in N_2 atmosphere on polycrystalline samples of complex **1**–**10** and the TG curves are shown in Figure S3. For complex **1**, the first loss at about 113°C is consistent with the removal of lattice water (obsd. 4.1%, calcd. 3.5%). The water-free network does not decompose until 230°C, and then the collapse of the network of **1** occurs. For complexes **2** and **3**, the isomorphic structure of complex **1**, the networks begin to collapse at about 210°C (for **2**), and 190°C (for **3**), finally given a result of thermal decomposition. For complex **4**, the weight loss below 170 °C can be attributed to the release of free and coordinated water molecules (obsd: 10.9%; calcd: 11.1%). The abrupt weight loss corresponding to the release of organic ligands starts at around 270 °C. For Complex **5**, the whole structure began to collapse over 315°C after the release of coordinated water molecules (obsd: 3.7%; calcd: 3.3%) in the temperature range of 75–115 °C. For complex **6**, the weight loss from 90 to 135 °C is attributed to the release of water molecules (obsd: 7.9%; calcd: 8.3%). Above 270 °C, it starts to lose its ligands a result of thermal decomposition. For complex **7**, two stages of weight occurred at 180 and 310°C, the organic ligands are gradually lost with a result of thermal decomposition. For complex **8**, the first two weight loss at 105 and 165 °C are attributed to the release of lattice water molecules (obsd. 4.9%; calcd. 5.2%) and methanol molecules (obsd. 9.6%; calcd. 9.3%). Then the collapse of the network of complex **8** occurs. For complex **9**, the weight loss below 150 °C can be attributed to the release of free and coordinated water molecules (obsd. 11.2%; calcd. 10.5%). The weight loss corresponding to the release of organic ligands starts at 225°C. The water molecules in compound complex **10** released at about 115 °C (obsd. 11.2%; calcd. 10.5%), and then it starts to gradually lose its ligands with a result of thermal decomposition.

Magnetic Properties. Temperature dependence of $\chi_M T$ for complex **4** is displayed in Figure S4. The $\chi_M T$ values for **4** at room temperature are 2.86 cm^3 K mol^{-1}, which are larger than an uncoupled (1.87 cm^3 K mol^{-1}) but smaller than that for two isolated Co^{II} cations (3.75 cm^3 K mol^{-1}), which can be attributed to the contribution to the susceptibility from orbital angular momentum at higher temperatures. In complex **4**, the Co···Co distance through the 4,4'–bibp bridge is 17.924 Å, and the $bcpb^{2-}$ ligand separated distances are 12.303 Å and 11.976 Å, respectively. The long Co···Co distances exclude an efficient direct exchange between the Co(II) ions. Thus, complex **4** can be regarded as a dinuclear model from the magnetic viewpoint. The susceptibility data were fit with anisotropic dimeric mode of the S = 3/2 spin, and the leastsquares analysis gives J = -2.8 cm^{-1}. The fitting result of a negative value for J indicates that complex **4** has weak antiferromagnetic interaction between the nearest Co(II) ions. The fitting result is comparable with those reported Co(II) dinuclear coordination polymers.[19]

Conclusions

In summary, a series of 2D and 3D coordination polymers (CPs) were synthesized based on two trifunctional pyridine-dicarboxylate (H_2bcpb and H_2pip) and three (bis)imidazole bridging ligands (1,4–bmib, 4,4'–bibp, and 4,4'–bimbp) under hydrothermal conditions. Compounds **1**–**10** displayed diverse structural features from 2D layers to 3D frameworks, such as (3,4)–connected $(4\cdot7^2)(4\cdot7^5\cdot8^4)$ for **4** and (3,5)–connected $(4\cdot6\cdot8)(4\cdot6^4\cdot8^5)$ for **10**, which have never been documented to date. Structural comparison of these networks reveals that not only the length (l_p) and width (l_c) of the trifunctional pyridine-dicarboxylate but also the flexible and length of the (bis)imidazole bridging ligands have great effect on the final packing structures. With the length of the (bis)imidazole bridging ligands increasing, the longer separation of neighboring cations makes the trifunctional pyridine-dicarboxylate adopt more "open" coordination modes, and the overall structure owns a higher degree of interpenetration. Moreover, the more flexibility of (bis)imidazole bridging ligands could make the trifunctional pyridine-dicarboxylate more twisted and the final structure more complicated.

Acknowledgements

The work was supported by financial support from the Natural Science Foundation of China (Grant Nos. 21101097, 91022034, and 51172127), Natural Science Foundation of Shandong Province (ZR2010BQ023), and Qilu Normal University is acknowledged.

Notes

The authors declare no competing financial interest.

References

1 (a) M. O'Keeffe and O. M. Yaghi, *Chem. Rev.*, 2012, **112**, 675; (b) B. L. Chen, N. W. Ockwig, A. R. Millward, D. S. Contreras and O. M. Yaghi, *Angew. Chem. Int. Ed.*, 2005, **44**, 4745; (c) Y. Cui, Y. Yue, G. Qian and B. L. Chen, *Chem. Rev.*, 2012, **112**, 1126; (d) G. Férey and C. Serre, *Chem. Soc. Rev.*, 2009, **38**, 1380; (e) Z. Chen, R. Wang and J. Li, *Chem. Mater.*, 2000, **12**, 762; (f) M. Kim, J. F. Cahill, H. Fei, K. A. Prather and S. M. Cohen, *J. Am. Chem. Soc.*, 2012, **134**, 18082; (g) H. Fei, J. F. Cahill, K. A. Prather and S. M. Cohen, *Inorg. Chem.*, 2013, **52**, 4011.

2 (a) J. Luo, J. Wang, J. Li, Q. Huo and Y. Liu, *Chem. Commun.*, 2013, **49**, 11433; (b) Y. P. He, Y. X. Tan and J. Zhang, *Chem. Commun.*, 2013, **49**, 11323; (c) X. Y. Chen, V. T. Hoang, D. Rodrigue and S. Kaliaguine, *RSC Adv.*, 2013, **3**, 23935; (d) J. P. Zou, Q. Peng, Z. Wen, G. S. Zeng, Q. J. Xing and G. C. Guo, *Cryst. Growth Des.*, 2012, **12**, 3845; (e) Y. P. He, Y. X. Tan and J. Zhang, *Inorg. Chem.*, 2013, **52**, 12758; (f) Z. Han, J. Jiang, J. Lu, D. C. Li, S. Cheng and J. M. Dou, *Dalton. Trans*., 2013, **42**, 4777.

3 (a) F. Cao, S. Wang, D. Li, S. Zeng, M. Niu, Y. Song and J. Dou *Inorg. Chem.*, 2013, **52**, 10747; (b) X. T. Zhang, D. Sun, B. Li, L. M. Fan, B. Li and P. H. Wei, *Cryst. Growth Des.*, 2012, **12**, 3845; (c) J. B. Lin, W. Xue, B. Y. Wang, J. Tao, W. X. Zhang, J. P. Zhang and X. M. Chen, *Inorg. Chem*., 2012, **51**, 9423; (d) T. Liu, S. N. Wang, J. Lu, J. M. Dou, M. J. Niu, D. C. Li and J. F. Bai, *CrystEngComm*, 2013, **15**, 5476; (e) X. Zhang, L. Fan, W. Zhang, Y. Ding, W. Fan and X. Zhao, *Dalton. Trans*., 2013, **42**, 16562; (f) P. V. Dau and S. M. Cohen, *Chem. Commun.*, 2013, **49**, 6128.

4 (a) Y. Y. Tang, C. X. Ding, S. W. Ng and Y. S. Xie, *RSC Adv.,* 2013, **3**, 18134; (b) L. Zhang, J. Guo, Q. Meng, R. Wang and D. Sun, *CrystEngComm*, 2013, **15**, 9578; (c) J. Li, L. Li, J. Liang, P. Cheng, J. Yu, Y. Xu and R. Xu, *Cryst. Growth Des.*, 2008, **8**, 2318; (d) L. M. Fan, X. T. Zhang, D. C. Li, D. Sun, W. Zhang and J. M. Dou, *CrystEngComm*, 2013, **15**, 349; (e) J. J. Zhang, Y. Zhao, S. A. Gamboa and A. Lachgar, *Cryst. Growth Des.*, 2008, **8**, 172.

5 (a) Q. Yu, Q. Zhang, H. Bian, H. Liang, B. Zhao, S. Yan and D. Liao, *Cryst. Growth Des.*, 2008, **8**, 1140; (b) Y. B. Wang, Y. L. Lei, S. H. Chi and Y. J. Luo, *Dalton Trans.,* 2013, **42**, 1862; (c) W. Hong, H. Lee, T. H. Noh and O. S. Jung, *Dalton Trans.,* 2013, **42**, 11092; (d) P. V. Dau, K. K. Tanabe and S.M. Cohen, *Chem. Commun.*, 2013, **49**, 9370; (e) P. V. Dau, M. Kim and S. M. Cohen, *Chem. Sci.*, 2012, **4**, 601.

6 (a) N. L. Torad, M. Hu, Y. Kamachi, K. Takai, M. Imura, M. Naito and Y. Yamauchi, *Chem. Commun.*, 2013, **49**, 2521; (b) X. Ma, X. Li, Y. E. Cha and L. P. Jin, *Cryst. Growth Des.*, 2012, **12**, 5227; (c) H. L. Wang, K. Wang, D. F. Sun, Z. H. Ni and J. Z. Jiang, *CrystEngComm*, 2011, **13**, 279; (d) D. P. Zhang, H. L. Wang, L. J. Tian, J. Z. Jiang and Z. H. Ni, *CrystEngComm*, 2009, **11**, 2447; (e) J. Liu, Y. X. Tan, J. Zhang, *Cryst. Growth Des.*, 2012, **12**, 5164.

7 (a) X. Lin, I. Telepeni, A. J. Blake, A. Dailly, C. M. Brown, J. M. Simmons, M. Zoppi, G. S. Walker, K. M. Thomas, T. J. Mays, P. Hubberstey, N. R. Champness and M. Schröder, *J. Am. Chem. Soc*., 2009, **131**, 2159; (b) H. S. Choi and M. P. Suh, *Angew. Chem. Int. Ed*., 2009, **48**, 6865; (c) B. L. Chen, N. W. Ockwig, A. R. Millward, D. S. Contreras and O. M. Yaghi, *Angew. Chem. Int. Ed*., 2005, **44**, 4745; (d) J. Jia, X. Lin, C. Wilson, A. J. Blake, N. R. Champness, P. Hubberstey, G. Walker, E. J. Cussen and M. Schroder, *Chem. Commun.*, 2007, 840.

8 (a) J. M. Lim, P. Kim, M. C. Yoon, J. Sung, V. Dehm, Z. J. Chen, F. Wurthner and D. Kim, *Chem. Sci.*, 2013, **4**, 388; (b) F. Guo, F. Wang, H. Yang, X. L. Zhang and J. Zhang, *Inorg. Chem*., 2012, **51**, 9677; (c) D. R. Xiao Y. G. Li, E. B. Wang, L. L. Fan, H. Y. An, Z. M. Su and L. Xu, *Inorg. Chem.*, 2007, **46**, 4158; (d) S. N. Wang, R. R. Yun, Y. Q. Peng, Q. F. Zhang, J. Lu, J. M. Dou, J. F. Bai, D. C. Li and D. Q. Wang, *Cryst. Growth Des.*, 2012, **12**, 79.

9 (a) Y. S. Wei, K. J. Chen, P. Q. Liao, B. Y. Zhu, R. B. Lin, H. L. Zhou, B. Y. Wang, W. Xue, J. P. Zhang and X. Chen, *Chem. Sci.*, 2013, **4**, 1539; (b) F. Wang, X. Jin, B. Zheng, G. Li, G. Zeng, Q. Huo and Y. Liu, *Cryst. Growth Des.*, 2013, **13**, 3522; (c) Q. Zhai, Q. Lin, T. Wu, S. Zheng, X. Bu and P. Feng, *Dalton. Trans*., 2012, **41**, 2866; (d) J. Jia, X. Lin, C. Wilson, A. J. Blake, N. R. Champness, P. Hubberstey, G. Walker, E. J. Cussen and M. Schroder, *Chem. Commun.*, 2007, 840.

10 (a) A. Phan, C. J. Doonan, F. J. Uribe-Romo, C. B. Knobler, M. O'Keeffe and O. M. Yaghi, *Acc. Chem. Res.*, 2010, **43**, 43; (b) W. Morris, C. J. Stevens, R. E. Taylor, C. Dybowshi, O. M. Yaghi and M. A. Garcia-Garibay, *J. Phys. Chem. C*, 2012, **116**, 13307; (c) T. F. Liu, J. Lu, X. Lin and R. Cao, *Chem. Commun.*, 2010, **46**, 8439; (d) Z. J. Lin, T. F. Liu, B. Xu, L. W. Han, Y. B. Huang and R. Cao, *CrystEngComm*, 2011, **13**, 3321; (e) L. F. Ma, M. L. Han, J. M. Qin, L. Y. Wang and M. Du, *Inorg. Chem.*, 2012, **51**, 9431.

11 (a) Z. Su, J. Fan, M. Chen, T. Okamura and W. Y. Sun, *Cryst. Growth Des.*, 2011, **11**, 1159; (b) D. B. Shi, Y. W. Ren, H. F. Jiang, B. W. Cai and J. X. Lu, *Inorg. Chem.*, 2012, **51**, 6498; (c) L. F. Ma, L. Y. Wang, Y. Y. Wang, S. R. Batten and J. G. Wang, *Inorg. Chem.*, 2009, **48**, 915.

12 (a) Y. Y. Lv, Y. Qi, L. X. Sun, F. Luo, Y. X. Che and J. M. Zheng, *Eur. J. Inorg. Chem.*, 2010, 5592; (b) H. Qu, L. Qiu, X. K. Leng, M. M. Wang, S. M. Lan, L. L. Wen and D. F. Li, *Inorg. Chem. Commun.*, 2011, **14**, 1347; (c) P. S. Wang, C. N. Moorefield, M. Panzer and G. R. Newkome, *Chem. Commun.*, 2005, 4405; (d) Y. L. Lu, J. Y. Wu, M. C. Chan, S. M. Huang, C. S. Lin, T. W. Chiu, Y. H. Liu, Y. S. Wen, C. H. Ueng,;T. M. Chin, C. H. Hung and K. L. Lu, *Inorg. Chem.*, 2006, **45**, 2430; (e) http://www.topos.samsu.ru.

13 (a) X. T. Zhang, L. M. Fan, X. Zhao, D. Sun, D. C. Li and J. M. Dou, *CrystEngComm*, 2012, **14**, 2053; (b) X. T. Zhang, L. M. Fan, Z. Sun, W. Zhang, D. C. Li, J. M. Dou J. M. and Han, L. *Cryst. Growth Des*., 2013, **13**, 792; (c) X. T. Zhang, L. M. Fan, W. Zhang, Y. S. Ding, W. L. Fan, L. M. Sun, X. Zhao and H. Lei, *Cryst. Growth Des*., 2013, **13**, 2462; (d) X. T. Zhang, L. M. Fan, Z. Sun, W. Zhang, D. C. Li, P. H. Wei, B. Li and J. M. Dou, *J. Coord. Chem.*, 2012, **65**, 3205; (e) L. M. Fan, X. T. Zhang, Z. Sun, W. Zhang, D. C. Li, P. H. Wei, B. Li and J. M. Dou, *J. Coord. Chem.*, 2012, **65**, 4389; (f) X. T. Zhang, L. M. Fan, Z. Sun, W. Zhang, D. C. Li, P. H. Wei, B. Li, G. Z. Liu and J. M. Dou, *Chinese J. Inorg. Chem.*, 2012, **28**, 1809; (g) Z. Sun, Y. S. Ding, L. J. Tian and X. T. Zhang, *J. Coord. Chem.*, 2013, **66**, 763.

14 (a) Bruker, SMART and SAINT (Bruker AXS Inc, Madison, Wisconsin, 2007); (b) G.M. Sheldrick, *Acta Cryst.* 2008, **A64**, 112.

15 V. A. Blatov, Struct. Chem. 2012, **23**, 955.

16 (a) R. Patra, H. M. Titi and I. Goldbery, *CrystEngComm*, 2013, **15**, 7257. (b) H. Li, Y. Han, X. Lv, S. Du, H. Hou and Y. Fan, *CrystEngComm*, 2013, **15**, 3672. (c) H. Zhou, G. Liu, X. Wang and Y. Wang, *CrystEngComm*, 2013, **15**, 1377.

17 (a) Hoboken, *Infrared and Raman Spectra of Inorganic and Coordination Compounds, Applications in Coordination, Organometallic, and Bioinorganic Chemistry* (Wiley, NJ, USA, 2009); (b) G. Mehlana, S. A. Bourne, G. Ramon and L. Ohrstrom, *Cryst. Growth Des*., 2013, **13**, 633; (c) D. Martini, M. Pellei, C. Pettinari, B.W. Skelton and A. H. White, *Inorg. Chim. Acta*, 2002, **333**, 72.

18 C. F. Macrae, P. R. Edgington, P. McCabe, E. Pidcock, G. P. Shields, R. Taylor, M. Towler and J. V. D. Streek, *J. Appl. Cryst.*, 2006, **39**, 453.

19 (a) X. J. Li, Y. Z. Cai, Z. L. Fang, L. J. Wu, B. Wei and S. Lin,*Cryst. Growth Des.*, 2011, **11**, 4517; (b) L. F. Ma, L. Y. Wang, M. Du and S. R. Batten, *Inorg. Chem.*, 2010, **49**, 365; (c) F. P. Huang, J. L. Tian, W. Gu, X. Liu, S. P. Yan, D. Z. Liao and P. Cheng, *Cryst. Growth Des.*, 2010, **10**, 1145; (d) A. Banisafar, D. P. Martin, J. S. Lucas and R. L. LaDuca, *Cryst. Growth Des.*, 2011, **11**, 1651.

CrystEngComm

For Table of Contents Use Only

Table of Contents Graphic and Synopsis

Syntheses, Structures, and Properties of A Series of 2D and 3D Coordination Polymers Based on Trifunctional Pyridine-dicarboxylate and Different (Bis)imidazole Bridging Ligands

Liming Fan, Xiutang Zhang, Wei Zhang, Yuanshuai Ding, Weiliu Fan, Liming Sun, Xian Zhao

Hydrothermal reactions based on two trifunctional pyridine-dicarboxylate carboxylates (H_2bcpb, H_2pip) and transitional metal cations in the presence of three (bis)imidazole bridging ligands (1,4-bmib, 4,4'-bibp, 4,4'-bimbp) afford ten 2D and 3D coordination polymers. Compounds **1**-**10** displayed diverse structural features from 2D layers to 3D frameworks, such as the binodal (4,4)-connected 3D framework of **7**, and trinodal (4,4,5)-connected 3D framework of **9**.